RESEARCH ARTICLE

A HYBRID DEEP LEARNING APPROACH FOR GROUND OBJECT INFORMATION EXTRACTION FROM HYPERSPECTRAL IMAGES

Gill Ammara[1], Hongwei Zhang[2], Chang-hua LIU[3] and Xiaojun NIE[4]
1. School of Surveying and Land Information Engineering, Henan Polytechnic University, Jiaozuo 454003, China.
2. School of Civil Engineering, Henan Polytechnic University, Jiaozuo 454000, China.
3. School of Surveying and Land Information Engineering, Henan Polytechnic University, Jiaozuo 454003, China.
4. School of Surveying and Land Information Engineering, Henan Polytechnic University, Jiaozuo 454003, China.

....

Manuscript Info
....

Abstract
....

Ground object information extraction out of hyperspectral images refers to the process of identifying and characterizing different materials or objects present on the earth's exterior using hyperspectral imaging technology. Hyperspectral imaging captures images in hundreds of small and adjacent spectral bands, providing more detailed and accurate information about the materials present in the scene. Hyperspectral data is high-dimensional, which can make it challenging to visualize and analyze. This can make it difficult to identify patterns or trends in the data, and can also make it challenging to interpret the results of classification algorithms. In this research work, collected raw images (GIS images) are pre-processed via Augmented median filtering and CLAHE approach. From the pre-processed images, the features like; Haralick features, Normalized Difference Vegetation Index (NDVI), Standardized Vegetation Index (SVI), correlation coefficient, Green-NDVI (GNDVI), Simple Ratio (SR), and Red-edge Simple Ratio (SRre) based features are extracted. Among the extracted features, the optimal features are preferred utilizing a new hybrid optimization model stated to as Wingsuit Spotted Hyena Optimizer (WSHO) model. This WSHO model is the conceptual blend of standard Wingsuit Flying Search (WFS) and Spotted Hyena Optimizer (SHO) Mineral Exploration phase is modelled with a three-fold-deep-learning-classifiers framework (proposed). The threefold-deep-learning-classifiers framework encapsulates the Support Vector Machine (SVM), Random Forest (RF), and modified Bi-LSTM. SVM and RF are trained with the selected optimal features acquired from WSHO. The outcome from SVM and RF is fed as input to Modified Bi-LSTM. To further enhance the detection accuracy, the loss function of Bi-LSTM is modified. The proposed model is implemented by PYTHON and validated in terms of various performance metrics.

....

Corresponding Author:- Gill Ammara
Address**:-** School of Surveying and Land Information Engineering, Henan Polytechnic University, Jiaozuo 454003, China.

Introduction:-

Ground remote sensing technology also encompasses the employment of numerous techniques to acquire detailed information of nearly all aspects concerning earth system that includes its status and occurrences to study the laws that govern it [1]. Hyperspectral sensing technology is one of the primaries means of earth observation technology or sometimes called as eyes for humans to venture out-for space exploration. The ground satellite orbit height is about 565 meters and the flight height of remote sensing aerial photography aircraft is about 10 km. 448 miles of airtime would have been needed for real-time collection of abundance data [2]. It should be noted that the scope of human examination in the extent of spectrum has expanded, and the structural point of data capturing has risen as hyperspectral image sensing earth surveillance technology became progressively established during the 1970. It has applied widely in agriculture, mining, military, water and soil conservation and the protection of the environment.

On the Earth there are a lot of regions with very complex environmental conditions; there are deserts and bogs, high mountains which are almost difficult for humans to access. Moreover, other methods of remote sensing, especially thermosphere ones, are faster and more effective in terms of data acquisition when it is impossible to conduct observations on the Earth's surface. Thermal infrared remote sensing shows the characteristic of higher spectral determination and higher spatial resolution, while the optical remote sensing holds a significant place in the development of remote sensing technologies [3][4]. Hyperspectral remote sensing satellites may capture images in several bands where each band possesses its characteristics. They work at a higher VNB resolution that is more readable, and are able to distinguish plants and water sources in the near-IR; whereas in the low-wave IR they are less sensitive to settings and in the thermal-IR they are useful for exterior humidity measurements [5]. Hyperspectral remote sensing has evolved into one of the key study paths in the field of remote sensing due to the ongoing increase of sensor spectral resolution and the broadening of individuals awareness of the spectral properties of ground items [6]. It blends spectroscopy technology with imaging technology. For the created remote sensing data to be brightly characterized by "image cubes," it disperses each spatial pixel even though imaging the spatial attributes of the target into tens or still hundreds of small bands for ongoing spectral scope [7][8][9].The acquired image is richer in spatial, emission, and spectral triple specifics than standard remote sensing techniques, and it is better able to differentiate between ground objects. Getting higher-resolution photos is the basic idea behind ground feature extraction. Technology assistance for quick and right capture of shifts in mining regions is made possible by the accelerated growth of remote sensing techniques [10]. To collect information about ground objects, hyperspectral remote sensing fuses spectral data with dimensional images. This enables the inclusion of maps and offers a persistent specialized foundation for humans to comprehend and change the universe. Compared to multispectral photos, hyperspectral images have a better resolution.

Image data acquiring through RS satellites is sensitive to weather, terrains, and other objectives; thus, it becomes almost impossible to monitor feature news of the objects on the ground within a small region especially in mining sites characterized with complex relief. Efficient approaches to mining ground material are being designed because of the enhancement in deep learning (DL) technology and speed of computers. It has been earlier observed in [11][12] that DL-based ground object information extraction is more accurate. Also, self-learning from the network of ground object properties reduces the amount of manual work and improves efficiency. In this case, temperature from thermal infrared hyperspectral data is and used as the classification criterion for the Jiaozuo Jiulishan mine situated in Jiaozuo City, China. The Convolutional Neural Network (CNN) under the DL is then applied to extract the ground characteristics in the mining area. This network has stronger generalization ability and higher recognition genuineness, which can be used to rapidly identify the ground characteristics of the mining area [13][14][15]. To ensure a shortage of a labeled sample when it comes to the training of the network model, the creation is extended whereby labeled data of other classifications from other datasets are obtained.

Motivation

- Hyperspectral imaging (HSI) is an efficient remote sensing technology, offering a wealth of spectral data across a broad range of wavelengths. This potential has inspired the use of HSI to detect and identify various ground objects. However, several challenges hinder the effective extraction of ground object information from hyperspectral images. However, hyperspectral data is characterized by high dimensionality and high volume, which creates storage, processing, and analysis problems. Heires identifies those conventional approaches can be highly ineffective when processing such intricate data.
- Usually, hyperspectral images consist of a high number of spectral bands, and a considerable portion of bands may be noisy or non-informative about the classification issue at hand. This redundancy may cause reduced accuracy of the classification and an increase in the computational load. Need for

Accurate Classification: The correct classification of ground objects is crucial for various applications, including monitoring environmental changes, agricultural productivity, mineral exploration, and military surveillance.

● However, previously used classification procedures have shown to be ineffective regarding precision and solidity, underscoring the importance of your work in these fields. Optimization of Feature Selection, effective feature selection is the primary condition that brings higher classification performance. However, selecting the best subset of features for the hyperspectral data is still difficult due to the large search space.

Main Contribution

• The new Wingsuit Spotted-Hyena Optimizer (WSHO) algorithm integrates the benefits of the Wingsuit Flying Search (WFS) and Spotted Hyena Optimizer (SHO) algorithms to select the best number of features from hyperspectral data.

• This approach to feature selection affirms the benefits mentioned above and combines the intensive approaches to feature selection. The set of optimal features is employed to train state-of-the-art classifiers, such as Support Vector Machine (SVM) and Random Forest (RF).

• These classifiers' results are, in turn, combined with an improved version of the Bi-LSTM network to enhance the classification results. The described model is developed in Python, and based on the results of testing with the use of the most significant parameters and indices, it is stated that the classification and prediction problems' solution with the help of the proposed model allows for providing higher accuracy, better performance, and less sensitivity to noise as compared with traditional approaches and tools.

• To illustrate the efficiency of the proposed model, it is implemented as a case of mineral exploration for the classification of different kinds of minerals extracted from hyperspectral images. This application emphasizes the analytical use of the model in solving real-life problems.

Research Questions

1). How the Wingsuit-Hyena Optimizer system can be used in improving the selecting of optimal features from the hyperspectral images compared to ancient characteristics of the methods selected.

2). What the particular modifications to the Bi-LSTM loss function should be for the enhancement of detection accuracy of the model proposed?

How should the proposed methodology function in the real-world application involving performance, and sensitivity metrics?

3). What are the core challenges in the extraction of object information from the hyperspectral images in the surrounding with complexity of terrains and how does the proposed methodology explore the outlined challenges?

4). How should the proposed model help in comparing with the existing hyperspectral images classification models in terms of computational efficiency and classification accuracy?

Literature Review:-

The developments in hyperspectral sensing as well as analysis over the years have proved to be very successful in many areas. Maximilian Brell et al. (2019) extended Hyperspectral Point Cloud (HSPC) by including preliminary pulse return information from ALS and suggested its feasibility for environmental and landcover classification [16]. Zhuo Zheng et al. (2020) proposed a hyper-scale object detection framework called HyNet based on a new block, called HyBlock, to optimize the crucial MSR images [17]. In this regard, based on the study by Radhesyam Vaddi et al. (2020), this research recommends the ONR approach for unsupervised band selection, alongside the SPRF and CNN for efficient data classification [18].

Street picture analysis and main studies on pictures in urban environment were carried out by Jianya GONG et al (2019) to highlight the methods from fundamental sections to more refined aspects and possible advancements in urban planning and large quantities of data [19]. Yi Liu et al., (2020) presented an algorithm linking the sparse illustration with the spectral, spatial and temporal factor of the RS images focusing on temporal characteristics and a model for sparse representation of space-spectrum-time [20].

A. Gokila Vani et al. (2020) involves is the segmentation of the surface characteristics in the form of images captured through satellite wherein the researchers' combined developments in hyperspectral sensors to capture data from

several hundred bands [21]. Muhammad Mahtab Alam et al. (2016) described a WBANs with dynamic MAC with latency and energy efficient protocol for randomly varying traffic load [22].

There is a process of hyperspectral image classification as Zhang et al. (2022) called nested transformers (NesT) that helps in better extraction of required information and to use on four commonly used hyperspectral databases [23]. Renlong Hang et al. (2019) proposed an HSI grading model based on attention-aided CNN, which include two subnetworks, spectral attention, and spatial attention [24]. Yanhui Guo et al. (2018) presented a novel structure based on CNN to implement the deep feature extraction and spectral-spatial classification for the multiscale spatial information [25-29].

The main contributions of this research include:
• Added augmented median filtering as the pre-processing method extension.
• Applying the methodology based on the Wingsuit Spotted-Hyena Optimizer for the feature selection.
• Utilizing Modified Bi-LSTM on the basis of outputs of high efficiency from the SVM and RF classifiers.

Section 3 describes the methodology of ground object information extraction from hyperspectral images and Section 4 contains the findings obtained with the help of the proposed model. Section five of the paper draws the conclusion.

Muhammad mahtab alam et al. [22] have proposed a wireless body area network (WBANs) where the wake-up schedule of the nodes has been changed in 2016. The developed protocol for dynamic MACwas latency-energy-optimized and traffic-aware. The said protocol was developed based on an adaptive algorithm that would allow the sensor nodes to have a good control of its wake up and sleep patterns depending on the traffic that is static and dynamic in nature.

Wang & Gan [3] presented a HSI classification process using nested transformers. The block aggregation component was applied by NesT to gather the edge information across patches and facilitate the outsiders' information exchange across blocks and enhance the overall information acquirement. The NesT was used for the characterization of the HSI for the first attempt. Four datasets in hyperspectral are selected which are most commonly used.

Renlong Hang et al. [24] have introduced a hyperspectral image grade in 2019 with the help of the attention-aided CNN model. To promote spectral and spatial classifications, two subnetworks are proposed: the spectral attention subnetwork and the spatial attention subnetwork. Based on the conventional CNN model, both of them contain attention modules; Specifically, support networks that focus on more discriminative channels are integrated into CNN architecture. In 2018, Yanhui Guo et al. [25] have used a High-efficiency deep feature extraction and the spectral-spatial HSI classification approach that can probably develop the multiscale spatial feature obtained by the guided filter. This was the initial demonstration of CNN in learning of spectral and multi-scale spatial information and was the suggested technique. Hence when it is so compared with its commercial rivals.

The following are some of the objectives that this research seeks to achieve with regards to the gaps that were defined when undertaking this research:

To begin with, it has a concise statement of motivation and main contribution; a rigorous presentation which has contributed the to the specification of an actuality hybrid model concerning ripping off the ground object information from hyperspectral images based on the WSHO and deep learning approaches. Secondly, we discussed the changes made to the Bi-LSTM and the research proposed hybrid model, so that readers can understand the difference and how our work is better than the base models. This involved changes in the loss function and the incorporation of outputs of Support Vector Machine (SVM) as well as Random Forest (RF) into the Bi-LSTM path. Thirdly, to alleviate the previously mentioned lack of information about the dataset samples used, we stated and explained the numbers of samples in training, testing, and validation datasets and the selected dataset splitting approach. It was quite important in the process of verifying the reliability and stability of the developed model. Below is the code that shows the computation and comparison of Performance Metrics Precision, Sensitivity, Specificity, F-Measure, MCC, NPV, FPR, FNR in WFS, SHO, SVM, Bi-LSTM, and the proposed model. This approach guarantees: elaboration of the rationale for each contribution, clear demonstration of the introduced modifications to the model, and scrupulous description of the dataset's handling, thereby increasing the comprehensibility and effectiveness of the research conducted.

Research Gaps

Table 1:- Shows the research gaps of various existing work.

AUTHOR	AIM	METHODOLOGY	DRAWBACK
Maximilian Brell et al. [16]	Combining airborne laser scanning with hyperspectral imaging sensors to improve the extraction of object-based information	Hyper structural point cloud	It requires a high level of technical expertise
Zhuo Zheng et al. [17]	hyper-scale object detection network framework	feature pyramid network	High computational costs
Radhesyam Vaddi et al. [18]	To classify hyperspectral images.	Optimal neighboring reconstruction	May not be effectively distinguish between meaningful structures and noise
Jianya GONG et al. [19]	Improvements in the extraction of urban information from highresolution remote sensing images	High-resolution remote sensing imagery	Problems such as spectral heterogeneity, and disparity in HR images
YI LIU et al. [20]	Remote Sensing Image Information Extraction, and Target Recognition	image extraction and recognition network	difficult to develop.
A.Gokila Vani et al.[21]	Classification of Hyperspectral images using SVM approach	Support vector machine	ultra-high dimensionality of data
Muhammad mahtab alam et al. [22]	A Heuristic Self-Adaptive Medium Access Control for WBAN Systems with Limited Resources	Wireless Body Area Networks	low storage capacity
Zitong Zhang et al. [23]	Recursive Generators for Classifying Hyperspectral Images	Conventional machine learning and DL	With spectrum, it is impossible to attain good performance.
Renlong Hang et al. [24]	Classification of Hyperspectral Images Using Attention-Aided CNNs	Hyperspectral images	some domains can impact the performance of the model
Yanhui Guo et al. [25]	classification of spectral information features.	Spectral-Spatial Hyperspectral Image	wide gap in expectations

Problem Statements Section
Problem Statements
- **Inefficient Real-Time Data Collection in Remote Sensing:**
Ground remote sensing technologies, despite their advancements, face significant challenges in acquiring real-time, detailed data due to limitations in satellite and aerial photography capabilities. Current systems require extensive flight times and operational costs to collect comprehensive data over large areas.
- **Limited Scope of Hyperspectral Imaging in Complex Environments:**
The effectiveness of hyperspectral imaging is constrained in environments with complex terrains such as deserts, mountains, and inaccessible regions. This limitation hinders the comprehensive observation and monitoring of Earth's diverse environmental conditions using traditional remote sensing techniques.
- **Integration Challenges of Thermal Infrared Remote Sensing:**
While thermal infrared remote sensing offers higher spectral and spatial resolutions compared to optical methods, its integration with existing remote sensing technologies poses challenges. These challenges include optimizing data acquisition efficiency and enhancing the applicability of thermal infrared data for environmental monitoring and resource management.
- **Accuracy and Efficiency Gaps in Ground Object Information Extraction:**

The extraction of ground object information from remote sensing satellite images remains inaccurate and inefficient, particularly in mining sites characterized by complex terrains and environmental conditions. There is a critical need to develop more efficient approaches utilizing deep learning technologies to enhance the accuracy and speed of ground object identification and classification.

- **Data Labeling and Training Challenges in Deep Learning Models:**

The training of deep learning models for ground object classification faces challenges related to the availability and quality of labeled data. Current approaches are limited by the shortage of labeled samples specific to mining area characteristics, necessitating the extension of data sources and augmentation techniques to improve model training and generalization.

Proposed Methodology:-

Economic growth is influenced by the mining of coal and its use. In this regard, research is done on feature information extraction in the region to support production deployment and arrangement precisely and effectively in the mining area. Figure 1 shows the overall architecture of the proposed work.
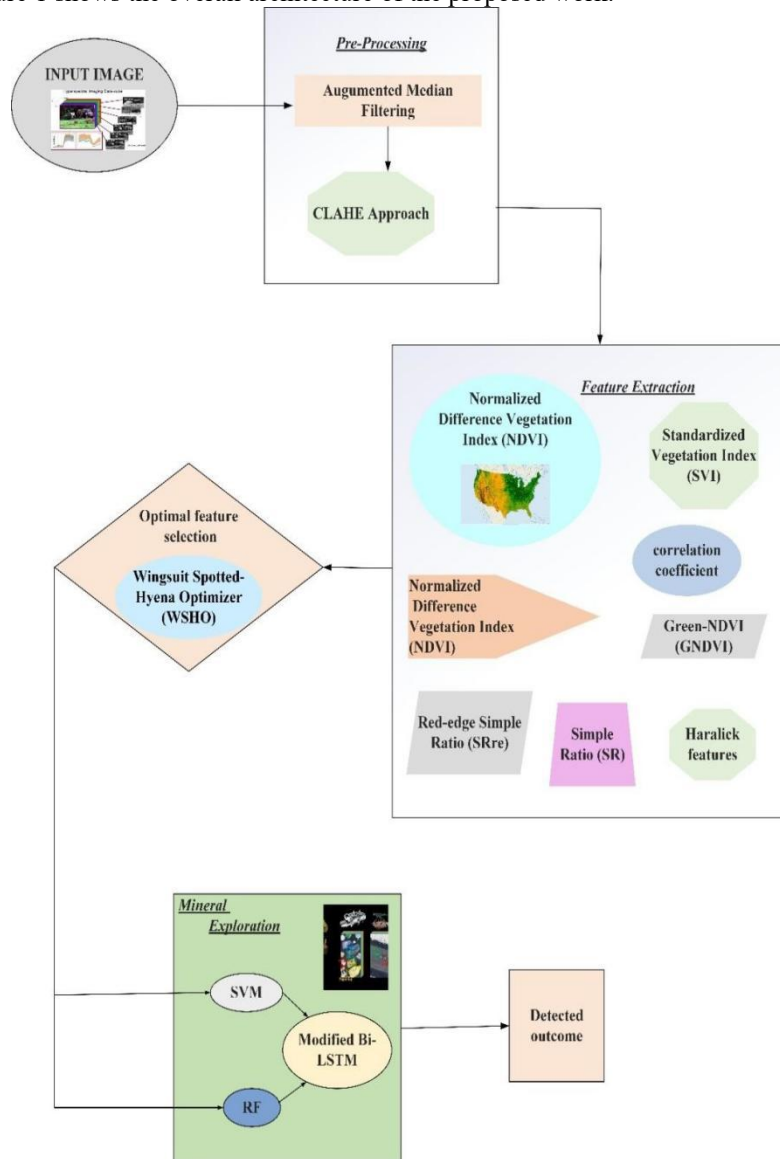
Figure 1:- Overall design of the proposed methodology.

Pre-processing:

The collected raw images (GIS images) is pre-processed via Augmented median filtering and CLAHE approach

Feature Extraction:
Then, from the pre-processed images, the features like Haralick features, Normalized Difference Vegetation Index (NDVI), Standardized Vegetation Index (SVI), correlation coefficient, Green-NDVI (GNDVI), Simple Ratio (SR), and Red-edge Simple Ratio (SRre) based features is extracted.

Optimal feature selection-
Among the extracted features, the optimal features is selected using a new hybrid optimization model referred as Wingsuit Spotted-Hyena Optimizer (WSHO) model (proposed). This WSHO model is the conceptual blend of standard Wingsuit Flying Search (WFS) [23] and Spotted Hyena Optimizer (SHO) [24], respectively.

Mineral Exploration-
This phase is modelled with a three-fold-deep-learning-classifiers framework (proposed). The three-fold-deep-learning-classifiers framework encapsulates the SVM, RF and modified Bi-LSTM (proposed). The SVM and RF is trained with the selected optimal features acquired from WSHO. The outcome from SVM and RF is fed as input to Modified Bi-LSTM. To further enhance the detection accuracy, the loss function of Bi-LSTM is modified.

Pre-processing
In this research work, Pre-processing is collected using raw images and it is processed using Improved median filtering(proposed) and CLAHE approach. Figure 2 shows the processes of Pre-processing.
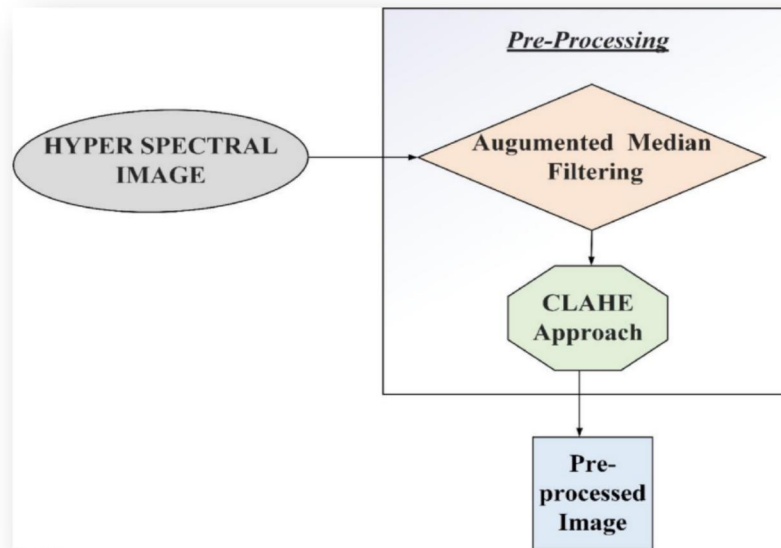

Figure 2:- Pre-processing phase.

Augmented median filtering
Augmented median filtering uses a variable window size based on the quality of the image data within the window. The window size is increased if the variation within the window exceeds a certain threshold, and it is decreased if the variation is below another threshold.

Mathematically, the Augmented median filter can be defined as follows:
Let (n, m) be the input image, and $y\,(n, m)$ be the output image after filtering. Let (p, q) be the window centered at pixel (n, p) in the input image, were
$p = n - [(w - 1)/2] \; to \; n + [(w - 1)/2],$

$q = m − [(w − 1)/2] \ to \ m + [(w − 1)/2].$ (1)

Let S be the size of the window, and Z_{min} and Z_{max} be the smallest and maximum intensity rates within the window.

Then the adaptive median filter is defined as follows:

Step 1: If $S<S_{mi}$, set $y(n, m) = Z_{med}$, the median value of the pixels within the window.

Step 2: If $Z_{min}<Z_{med} < Z_{max}$ set $(n, m) = x(n, m)$.

Step 3: If $S>Smax$, $set \ (n, m) = Zmed$.

Step 4: If $Smin<= S<= Smax$ and $Zmed<= ZminorZmed>= Zmax$, increase the window size by 2 and repeat the above steps.

If the window size exceeds a predefined maximum size, set $(n, m) = Zmed$ and move to the next pixel.

This approach allows for the preservation of important image details while removing noise and artifacts. The use of variable window sizes based on the attributes of the image data within the window ensures that important details are not lost during the filtering process.

CLAHE approach

The result of combining this limited contrast approach with the AHE results is the CLAHE, also known as the Contrast Limited Adaptive Histogram. Better images are mainly made when comparing interactive contrast enhancement to Adaptive Histogram Equalization (AHE). It served as proof that adding more shadows to the original image could lead to more effective results. It was noted that for an image with a constrained range of grey levels, AHE does not yield satisfactory results. Noise is decreased and improved images are produced by restricting contrast enhancement. The disadvantage of AHE is that it makes the image's noise and image quality worse. As a way to advance, the CLAHE was recommended. This method improves the image while lowering noise. According to the CLAHE strategy, First, the image is distributed into a number of nearly identical, non-overlapping regions. The histogram for everywhere is then calculated. The desired limit for contrast expansion is then used to determine a clip limit for clipping histograms. The height of each histogram is then readjusted to keep it within the clip limit. Eq. (2) is used to calculate the clip limit β.

$$\beta = \frac{BC}{W}\left(1 + \frac{\alpha}{100}(Z_{max} − 1)\right)$$ (2)

Where α is a clip factor, if clip factor equivalent to zero the clip limit becomes exactly equal to $\frac{BC}{W}$, additionally, if clip limit equals 100, the highest permitted slope is Z_{max}. The Cumulative Distribution Functions (CDF) of the resulting contrast limited histograms are then computed for use in grayscale mapping. The pixels are designed by linearly merging the results of the mappings of the four closest sections.

Feature Extraction

In this research work, the pre-processed images are fed up into feature extraction.

Feature extraction is done using Haralick Features, SR, NDVI, SVI, Correlation Coefficient, Green-NDVI (GNDVI) and Red-Edge Simple Ratio. Figure 3 shows the processes of Feature Extraction.
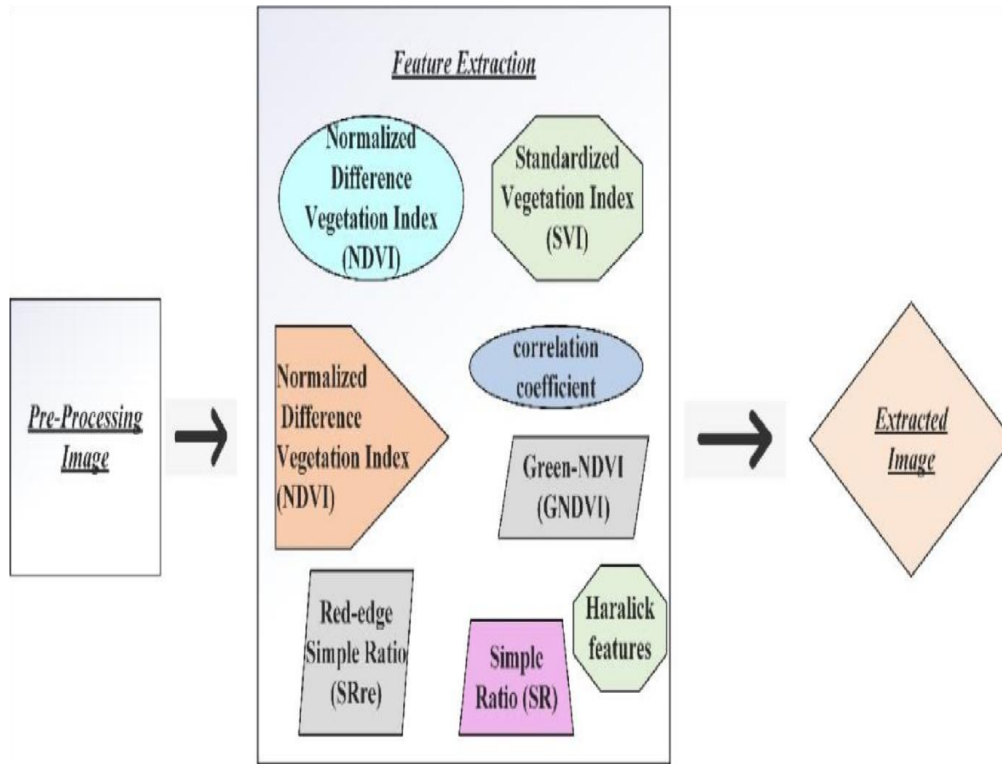
Figure 3:- Feature Extraction.

Haralick Features

Grey Level Co- Occurrence Matrix (GLCM) is a potent method for quantifying texture features. Consider a rectangular image that needs to be analysed, with V_a columns and V_c rows. Assume that each pixel's grey level has been calculated to V_g tiers. Let, T_a= 1, 2, , V_a be the columns, T_c= 1,2,… , C_a be the rows, and Y=0 ,1, 2…, V_g be the set of V_g quantized grey levels. The texture-context information is stated by the matrix of relative frequencies $Q_{i,j}$ with two nearby pixels disconnected by deposition e and angle θ. The subsequent equation is used to calculate the GLCM that is mathematically shown in Eq. (3)

$$Q(i,j,e,\theta) = \#\{(a_1,c_1)(a_2,c_2)|m(a_1,c_1)=i, m(a_2,c_2)=j,|(a_1,c_2)-(a_2,c_2)|=e, ↓((a,c_1),(a_2,c_2))=\theta\} \qquad (3)$$

where $\#$ is the number of instances inwardly the window sizes where a pixel pair's intensity level variations from i to j, the first pixel's location is (a_1,c_1) the second pixel's location is (a_2,c_2) e is the span between the pixel pair, and is the angle separating certain two pixels. The defined co-occurrence matrix is non-symmetric. Only angles up to 180° must be considered when the GLCM is measured with symmetry. A symmetric co-occurrence matrix is estimated by the look $Q(i, j, e, \theta)' = (Q(i, j, e, \theta) + Q(i,j,e,\theta)^{DF})/2$ where $Q(i, j, e, \theta)^{DF}$ is the transpose of $Q(i, j, e, \theta)$. Probability estimates are collected by dividing each entry in $Q(i, j, e, \theta)'$ by the sum of all practicable intensity changes (DF_a*DF_c) with the distance e and management θ i.e. $\sum \# DF_a DF_c, e, \theta$ Thus, a normalized GLCM is obtained by the Eq. (4).

$$Q(i,j,e,\theta)^V = \frac{Q(i,j,e,\theta)+Q^{DF}(i,j,e,\theta)}{2*\sum \# DF_a DF_c, e, \theta} \qquad (4)$$

where, $Q(i, j, e, \theta)^V$ is normalized GLCM. $2 * \sum \# DF_a DF_c, e, \theta$ is constant and in order to elude division on the FPGA, the Eq. (4). can be rewritten as follows. Division uses more appliances resources and can reduce the functioning of the FPGA design. The mathematical model is shown in Eq. (5)

$$(i,j,e,\theta)^V = (Q(i,j,e,\theta)+Q^{DF}(i,j,e,\theta))*K(e,\theta) \qquad (5)$$

NDVI

$$X_{RSQ} = \frac{X_{RI}XRI - D_{er}DER}{X_{RI}XRI + D_{er}DER} \quad (6)$$

The NDVI is expressed mathematically in Eq. (6). The normalized difference vegetation index is X_{RSQ}. With sensors in the D_{er} and XRI regions, D_{er} and XRI are spectral radiance dimensions. The amount of energy flux that a sensor can detect is called radiation. Radiance values are frequently resizable to numeric numbers as unsigned 6-bit, 7-bit, 8-bit, or 12-bit integers. Reflectance is a unit less measurement of how much radiation an object reflects compared to how much radiation strikes it. No matter whether radiance, reflectance, or DN are used as inputs, NDVI range from 1 to 1. Its ethics are typically negative for vegetation, such as crops, shrubs, grasses, and forests, and close to zero for surfaces made of rocks, sand, or concrete.To put it another way, higher NDVI values have stronger implications for lush vegetation. To lessen the impact of scattered radiation in the atmosphere, reflectance is used. Shorter wavelengths scatter more strongly than longer wavelengths according to the Rayleigh scattering theory of strong wavelength dependence on dispersion in the air, which has an impact on NDVI calculations. The relative differences in spectral responses of various objects are what cause the variations in NDVI values between them. Consequently, Eq. (7) can be modified as follows.

$$X_{RSQ} = \frac{D-1}{D+1} \quad (7)$$

where X_{RSQ} is normalized dissimilarity vegetation index. D is the rate of XRI to D_{er}, and is generally cited as to ratio vegetation index? Eq. (7)is more exact for explaining NDVI behavior patterns due to separate responses of XRI and Red to atmosphere and stress.

SVI

The Z-score was used to determine the Standard Deviation (SD) from the mean in the unit of the SD, which was measured from the NDVI of each pixel in each season, because the SVI trusted on a z-score in each pixel of the data from the Terra/MODIS. The analysis of the z-score is depicted in Eq. (8).

$$Y_{cdf} = \frac{NDVI_{cdf} - \overline{NDVI}_{cd}}{\sigma_{cd}} \quad (8)$$

Were,

Y_{cdf} = the year f s pixel c's Y value for week d, $NDVI_{cdf}$= the per week NDVI value for pixel c through week d for annum f. $\overline{NDVI}_{cd}$= the mean NDVI for pixel c within week d above n years σcd = the SD of pixel c amid week d over n years.

According to Eq. (8), Y_{cdf} was the hypothesis value in order to correspond with the standard normal distribution for the test of the hypothesis from any pixel
in any season for the interval of 2014-2016. SVI analysis could be done as shown in Eq. (9)

$$SVI = \frac{(Y_{cdf} - Y_{cdMN})}{(Y_{cdMA} - Y_{cdMN})} \quad (9)$$

Were,

Y_{cdf} = the year f s pixel c's Y value for week d.
Y_{cdMA}= highest Y value for pixel c when week d and Y_{cdMN}= minimum of Y
value for pixel c during week d
Eq. (9) display of the probability of each pixel as the SVI.

Correlation Coefficient

The Pearson Correlation Coefficient (PCC) is a popular statistic for determining how much two image matrices R and G are linearly correlated.

GNDVI

Green Normalized Difference Vegetation Index. With the Exception of Measuring the Green Spectrum in the Range of 0.54 To 0.57 Microns Rather Than the Red Spectrum, it is Comparable to NDVI. According to Multispectral Data That Lacks an Extreme Red Channel,

This Serves as a Measure of the Photosynthetic Activity of the Vegetation Cover. It is More

Responsive to Chlorophyll Concentration Compared to the NDVI Index. When Evaluating Aged and Depressed Vegetation, it is Used. The mathematical model of GNDVI is shown in Eq. (10)

$$GNDVI = \frac{(NIR-GRN)}{(NIR+GRN)} \qquad (10)$$

SR
The SR is also well-known and frequently employed. It is specified as the ratio of red-light absorption to NIR light scattering. Mathematical model of SR is shown in Eq. (11)

$$SIMPLE\ RATIO = \frac{NIR}{RED} \qquad (11)$$

Red-Edge Simple Ratio (SRre)
An indicator of number of both healthy and distressed plants is the SRre method. The amount of light was spreading in the NIR and red-edge groups determines how much the effects of topography and atmosphere are reduced. The mathematical model of Red-Edge Simple Ratio is shown in Eq. (12).

$$SRre = \frac{NIR}{RedEdge} \qquad (12)$$

Optimal feature selection
In this research work, the extracted images are fed up into optimal feature selection. Optimal feature selection is done using Wingsuit Spotted Hyena Optimizer (WSHO). Figure 4 shows the process of optimal feature selection phase.
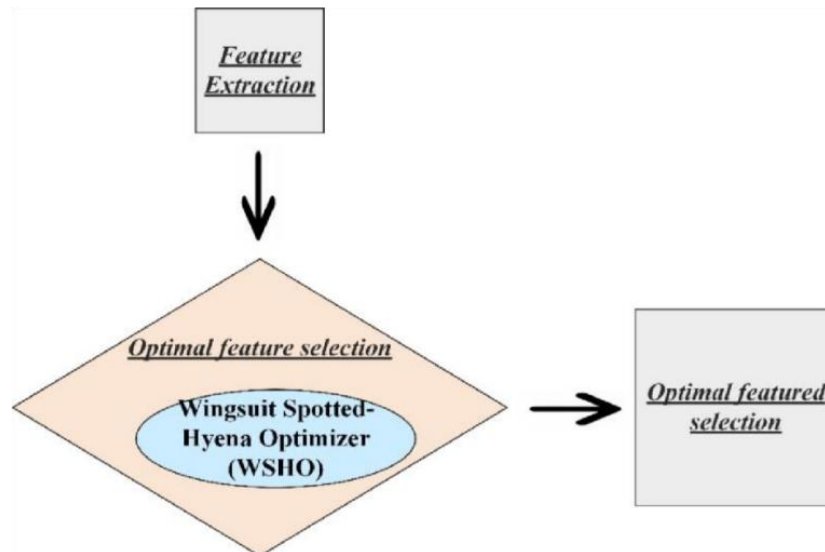
Figure 4:- Optimal feature selection phase.

Wingsuit Flying Search
The wingsuit flying search is implied with spotted Hyena Optimizer.
Step 1: Compute the spotted hyenas population.
Step 2: Determine the starting points of SHO.
Step 3: In this research work, calculate fitness function as given as fit=min (RMSE). Step 4: Find the most effective search agent in the available search space using the encircling prey phase.

The target prey is thought to be the best option at this time because the search space is unknown. Hyenas in the area that are searching for the target attempt to update their positions relative to it. This behavior can be mathematically expressed in Eq. (13) and Eq. (14)

$$\overrightarrow{Dis}_h = \left| \overrightarrow{A} . \overrightarrow{V}_{prey}(x) - \overrightarrow{V}_{hyena}(x) \right| \tag{13}$$

$$\overrightarrow{V}_{hyena}(x+1) = \overrightarrow{P}_{prey}(x) - \overrightarrow{C} . \overrightarrow{Dis}_h \tag{14}$$

Here, x is the current iteration, $\overrightarrow{A}$ and $\overrightarrow{C}$ are the coefficient vectors, $\overrightarrow{V}_{prey}(x)$ and $\overrightarrow{V}_{hyena}(x)$ are the position vectors of the prey and spotted hyena and the $\overrightarrow{Dis}_h$ is the? separation within the spotted hyena and prey. However, (.) and (‖) are the multiplication of vector and absolute value correspondingly. Eq. (15) - (17) shows the calculation for the vectors $\overrightarrow{A}$ and $\overrightarrow{C}$.

$$\overrightarrow{A} = 2 . r \overrightarrow{d_1} \tag{15}$$

$$\overrightarrow{C} = 2 \overrightarrow{h} . r \overrightarrow{d_2} - \overrightarrow{h} \tag{16}$$

$$\overrightarrow{h} = 5 - (Iteration * (\frac{5}{Max_{Iteration}})) \tag{17}$$

$Iteration = 1,2,3,\ldots,Max_{Iteration}$. $r\overrightarrow{d_1}$ and $r\overrightarrow{d_2}$ represents the random vectors. A dissimilar number of locations can be attained by varying the values of $\overrightarrow{A}$ and $\overrightarrow{C}$ vector.

Step 5: Specify the group of Optimal solutions based on the hunting phase of SHO model.

When hunting, hyenas typically rely on the information given by reliable associates and their propensity for tracking prey. The most effective search agent is the hyena that has the most knowledge of the location of its prey. In order to update their positions, additional search agents form a group and follow the best search agent. The mathematical model is shown in Eq. (18) – Eq. (20)

$$\overrightarrow{Dis}_h = \left| \overrightarrow{A} . \overrightarrow{V}_h - \overrightarrow{V}_k \right| \tag{18}$$

$$\overrightarrow{V}_k = \overrightarrow{V}_h - \overrightarrow{C} . \overrightarrow{Dis}_h \tag{19}$$

$$\overrightarrow{B}_h = \overrightarrow{V}_k + \overrightarrow{V}_{k+1} + \cdots \ldots + \overrightarrow{V}_{k+N} \tag{20}$$

Where $\overrightarrow{V}_h$ and $\overrightarrow{V}_k$ the positions of the first-best spotted hyena and other spotted hyenas, respectively. The count of spotted hyenas is indicated by N which is determined as in Eq. (21)

$$N = count_{nos}(\overrightarrow{V}_h, \overrightarrow{V}_{h+1}, \overrightarrow{V}_{h+2} \ldots \ldots, (\overrightarrow{V}_h + \overrightarrow{J})) \tag{21}$$

The total number of solutions after adding is symbolized by nos and $\overrightarrow{J}$ is a random vector in the extend [0.5, 1 and $\overrightarrow{B}_h$ is a collection of N optimal solutions.

Step 6: Generate the neighborhood points based on WFS.
Since it is a priori the ideal strategy to deal with an unknown environment, the flier really starts out placed above the center of the Earth surface of interest. Having a point that considers the flyer's present location is advantageous. This location, called the centroid by WFS, is identified as mathematical in Eq. (22)

$$g_1^{(m)} = \frac{\sum_{i=1}^{N^{(m)}+N} U^{(m)}(i) . \gamma \left(U^{(m)}(i) \right)}{\sum_{i=1}^{N^{(m)}+N} \gamma \left(U^{(m)}(i) \right)} \tag{22}$$

Where the columns are signified as $z(m)$ and $w_j \left(z_i^{(m)} \right)$. $U^{(m)}$ indicates pattern matrix in all points. Its dimensions are $n \times ((m) + N)$, and its ith column is indicated by $U^{(m)}(i)$.
For point x, the weighting factor (γ) is calculated as mathematical in Eq. (23)

$$\gamma(z) = \begin{cases} 1 - \frac{f(x) - f^{*(m)}}{a(m) - f^{*(m)}}, & f(x) \leq a(m) \\ 0, & f(x) > a(m) \end{cases} \tag{23}$$

Step 7: Exploitation

The value of $\vec{h}$ is gradually dropped from 5 to 0 at the time of exploitation. Additionally, the variation in $\vec{C}$ is also applied. The method allows the hyenas to attack the victim when the value becomes $\left|\vec{C}\right| < 1$. It can be stated in Eq. (24)

$$\vec{V}_{hyena}(x+1) = \frac{\vec{B}_h}{N} \tag{24}$$

Where $\vec{V}_{hyena}(x+1)$ is the best position record.

Step 8: In a given search space, determine if any search agents cross the boundary and make necessary adjustments.

Step 9: Create a value for the updated search agent fitness and update the $\vec{V}_k$ if a better option exists than the previous best option.

Step 10: Update on the spotted hyena pack B_h to revised fitness value for search agents.

Step 11: When the stopping criterion is met, algorithm come to a stop. If not, proceed to Step 5.

Step 12: Once the stopping criteria have been met, give the best optimal solution that has been found so far.

Mineral Exploration

In this research work, Optimal feature selection is fed up to mineral exploration phase. Mineral Exploration is processed through SVM and RF via Modified Bi-LSTM. Figure 5 shows the mineral exploration phase.
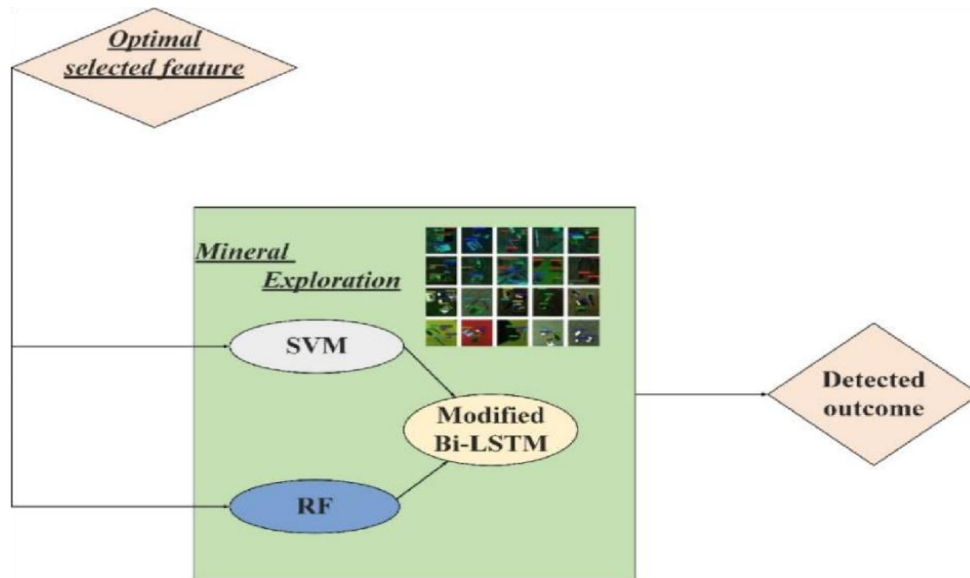
Figure 5:- Phases of Mineral Exploration.

Support Vector Machine (SVM)

SVM frequently used for regression analysis and classification. This classifier's main idea is to identify the negative samples and choose the best way to partition the positive samples. Training samples are used to develop trustworthy models, and both positive and negative examples are taken into account by the space points. The many types of points are represented by various forms and colours. There is a maximum of diversity with the assorted sample classes. Kernel function automatically converts the low-dimensional input features to features in a higher feature space.

Random Forest (RF)

A classification technique called Random Forest combines many tree predictors in such a way that each tree is dependent on a value of an arbitrarily selected vector that is equally circulated within all the trees in the forest. Since each tree is developed using the training set and random vector k, the RF creates a random vector θk that is

unrelated from the earlier random vectors θ_k and dispersed to entire trees. This produces a group of tree-structured classifiers $\{h(x, \theta_k), k = 1, \dots . \}$ at input vector x. The generalization error in the RF is mathematical shown in Eq. (25)

$PE^* = _{X,Y}(mg(X, Y) < 0)$ (25)

where margin function, mg, indicates how much the norm quantity of votes at random vectors for the right output outdo the average vote for any other output and subscripts X and Y are random vectors that denote the probability is over the X,Y space.

Highway-Bi-LSTM
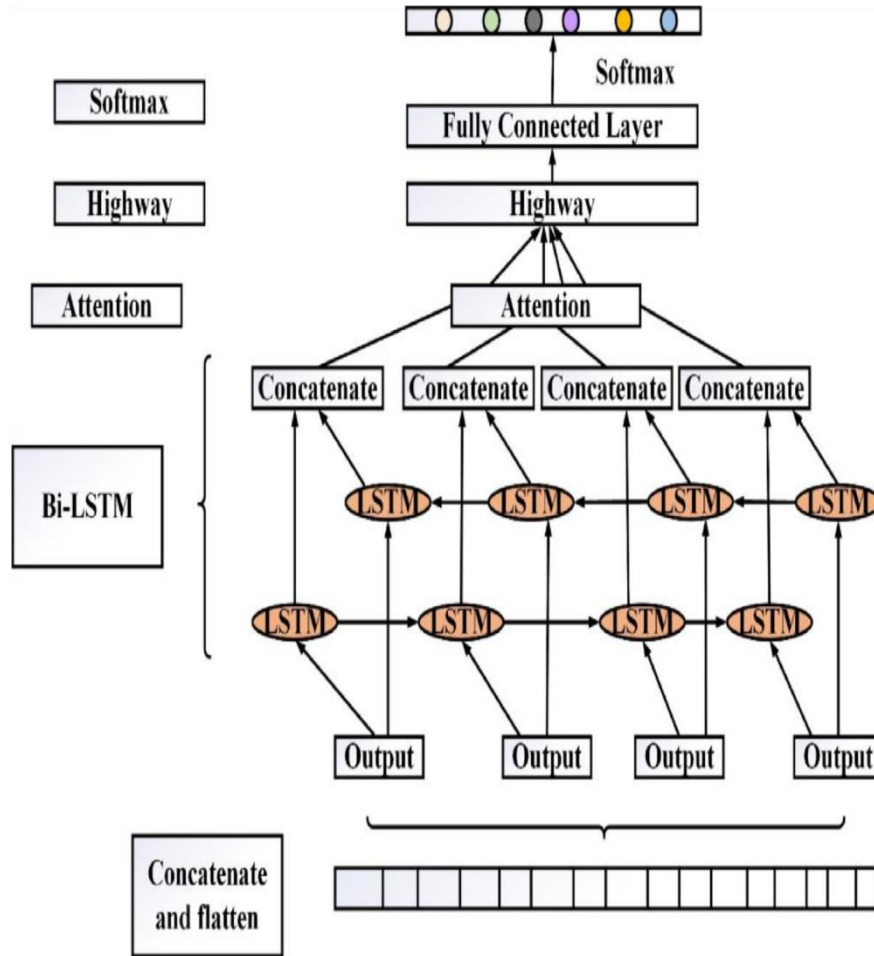
Figure 6:- Highway Bi-LSTM.

In a Highway-Bi-LSTM, highway layers are added to the standard Bi-LSTM architecture. The highway layer allows the network to learn when to carry information through the network and when to bypass it. Mathematically, a Highway layer can be defined as follows in Eq. (26) and Eq. (27).

$y = (x,WH) \backslash cdot\ T(x, WT) + x\ \backslash cdot\ (1 - T(x, WT))$ (26)

$y = H(x, WH) \cdot (x, W\ T) + x \cdot (1 - T(x, W\ T))$ (27)

Where x is the input to the layer, H is a non-linear transform function, T is a transform gate function, and WH and WT are the learnable weight parameters of the layer. The non-linear transform function H takes the input x and applies a non-linear activation function (e.g., ReLU) to it. This allows the layer to learn complex representations of the input. The transform gate function T takes the input x and applies a sigmoid activation function to it. This function outputs a value amongst 0 & 1 that represents the proportion of input that is carried through the layer (i.e., the "transform" part of the layer). The bypass gate $(1 - (x, WT)$ calculates the proportion of the input that is "bypassed" through the layer unchanged. This ensures that important features are not lost during the transformation process. The output y of the Highway layer is a combination of the transformed input and the bypassed input, with the proportion of each determined by the transform gate. Figure 6 shows the Highway Bi-LSTM representation.

Results and Discussion:-

The proposed model is implemented using PYTHON. The proposed model is analysed in terms of MCC, NPV, Sensitivity, recall, precision, specificity, F- score, FPR, FNR and accuracy.

- True Positive (TP) is a measure of how many positive class samples that correctly predicted.
- True Negative (TN) denotes the number of negative class samples that the algorithm correctly predicted.
- False Positive (FP) is a assess of how many samples from the opposing class that the model incorrectly predicted.
- False Negative (FN) suggests how many positive classes tries the algorithm predicted improperly.

Accuracy

The ratio of correct predictions to total predictions makes up the accuracy metric, one of the easiest Classification metrics to implement. Eq. (28) is the accuracy formula's mathematical representation.

$$Accuracy = \frac{TP+TN}{TP+FP+FN+TN} \quad (28)$$

Precision

The proportion of positive predictions that were accurate is determined by precision. It can be calculated as the True Positive, or the proportion of positive predictions that actually come true. The mathematical model is shown in Eq. (29).

$$Precision = \frac{TP}{FP+TP} \quad (29)$$

Sensitivity

The total positives divided by the proportion of actual positive forecasts yields the sensitivity value. The mathematical model is shown in Eq. (30).

$$Sensitivity = \frac{TP}{TP+FN} \quad (30)$$

Specificity

The percentage of accurately predicted negative outcomes over all negative outcomes is known as specificity. The formula for specificity is mathematically shown in Eq. (31).

$$Specificity = \frac{TN}{FP+TN} \quad (31)$$

F-Measure

It is computed as harmonic mean of both precision and recall, giving each variable equal weight. The formula for F-Measure is mathematically shown in Eq. (32).

$$F\_Score = \frac{Presision.Recall}{Presision+ Recall} \quad (32)$$

MCC

MCC is a trustworthy metric for evaluating the effectiveness of binary classifiers because it considers TP, TN, FN, and FP. MCC actually measures how closely the predictor and the actual labels are correlated. The formula for MCC is mathematically shown in Eq. (33).

$$MCC = \frac{(TP*TN)-(FP*FN)}{\sqrt{(TP+FP)(TP+FN)(FP+TN)(TN+FN)}} \quad (33)$$

NPV

A statistical measure known as Negative Predictive Value (NPV) assesses the reliability of a negative test result in a population of people who have an individual condition. It is considered by parting the total number of people without the condition by the count of true negative results. NPV is used to assess the effectiveness of detection. The formula for NPV is mathematically shown in Eq. (34).

$$NPV = \frac{TN}{TN+FN} \qquad (34)$$

FPR

The false positive rate is calculated by division the number of negative events that were inadvertently characterized as positive by the total sum of negative events. Formula for FPR is mathematically shown in Eqn. (35).

$$FPR = \frac{FP}{FP+TN} \qquad (35)$$

FNR

It is possible for a test to miss detecting a true positive, which is familiar as the false negative rate or "miss rate." The formula for FNR is mathematically shown in Eq. (36).

$$FNR = \frac{FN}{FN+TP} \qquad (36)$$

Table 2:- Performance Metrics of proposed and existing methodology.

	WFS	SHO	SVM	Bi-LSTM	Proposed
Accuracy	0.823974	0.838001	0.863093	0.831828	0.935071
Precision	0.789270	0.879402	0.855999	0.824981	0.927374
Sensitivity	0.866078	0.793823	0.870361	0.838823	0.942934
Specificity	0.782427	0.881594	0.855922	0.824926	0.927312
F-Measure	0.799202	0.809898	0.836210	0.805910	0.905936
MCC	0.829492	0.829906	0.901164	0.874601	0.983152
NPV	0.865542	0.804355	0.870331	0.838814	0.942923
FPR	0.024722	0.020224	0.026359	0.021711	0.020501
FNR	0.006623	0.004187	0.010017	0.003805	0.003593

The results in Table 2 shows the performance metrics of five different models: WFS, SHO, SVM, Bi-LSTM, and a proposed model. Accuracy of 0.935071 is achieved, indicating that it had the highest number of correct predictions. The proposed had highest precision of 0.927374, indicating that it had a high proportion of correct positive predictions. The proposed model achieved the highest sensitivity of 0.942934, indicating that it correctly identified the highest number of actual positives. The proposed model had a specificity of 0.927312, indicating that it correctly identified a high proportion of actual negatives. F-measure of 0.905936, indicating that it had the best balance between precision and sensitivity. The proposed model achieved the highest MCC of 0.983152, indicating a strong correlation between the predicted and actual classifications. NPV of 0.942923 of proposed, indicating that it correctly identified a high proportion of actual negatives among all predicted negatives. The proposed model had a relatively low FPR of 0.020501, indicating that it had a low proportion of false positives. The proposed model had the lowest FNR of 0.003593, indicating that it had the lowest proportion of false negatives. Overall, the proposed model performed significantly better than the other four models, achieving the highest values in most performance metrics. It achieved high accuracy, precision, sensitivity, specificity, F-measure, MCC, NPV, and low FPR and FNR values. Therefore, the proposed is the best among the five for the given task.
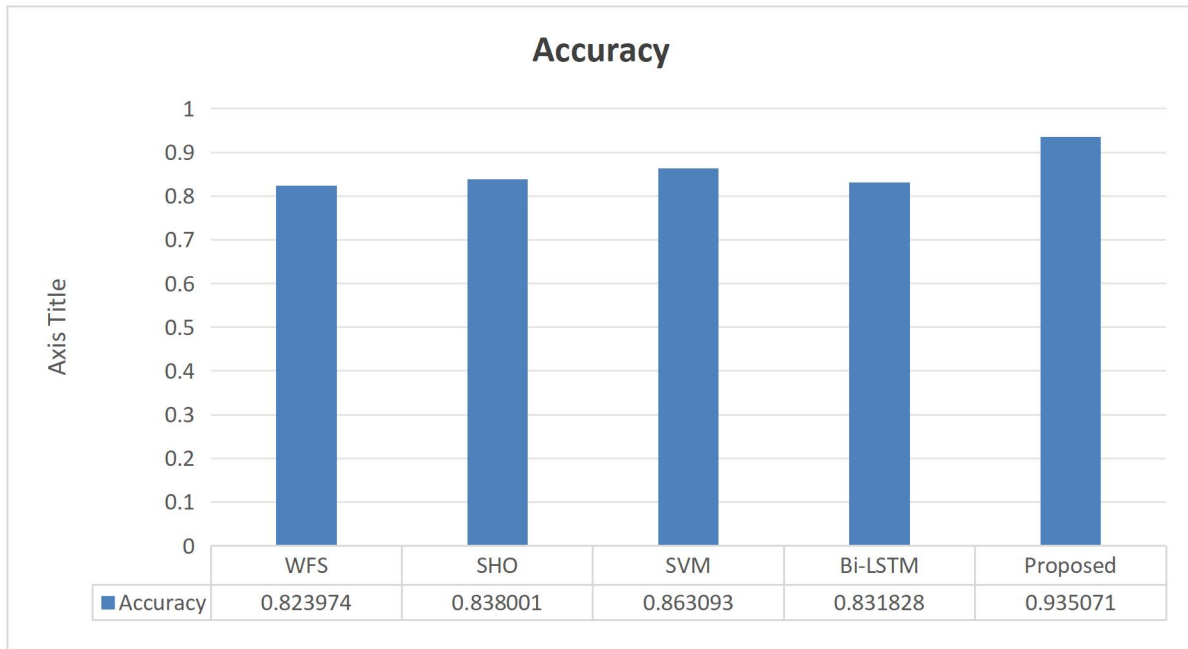
Figure 7:- Accuracy.

Figure 7 shows the accuracy analysis. The suggested scheme acquired the top score accuracy of 0.935071, indicating that it had the highest number of correct predictions. The SVM model also performed well, achieving an accuracy of 0.863093, while the WFS, SHO, and Bi-LSTM models had lower accuracy scores of 0.823974, 0.838001, and 0.831828, respectively.
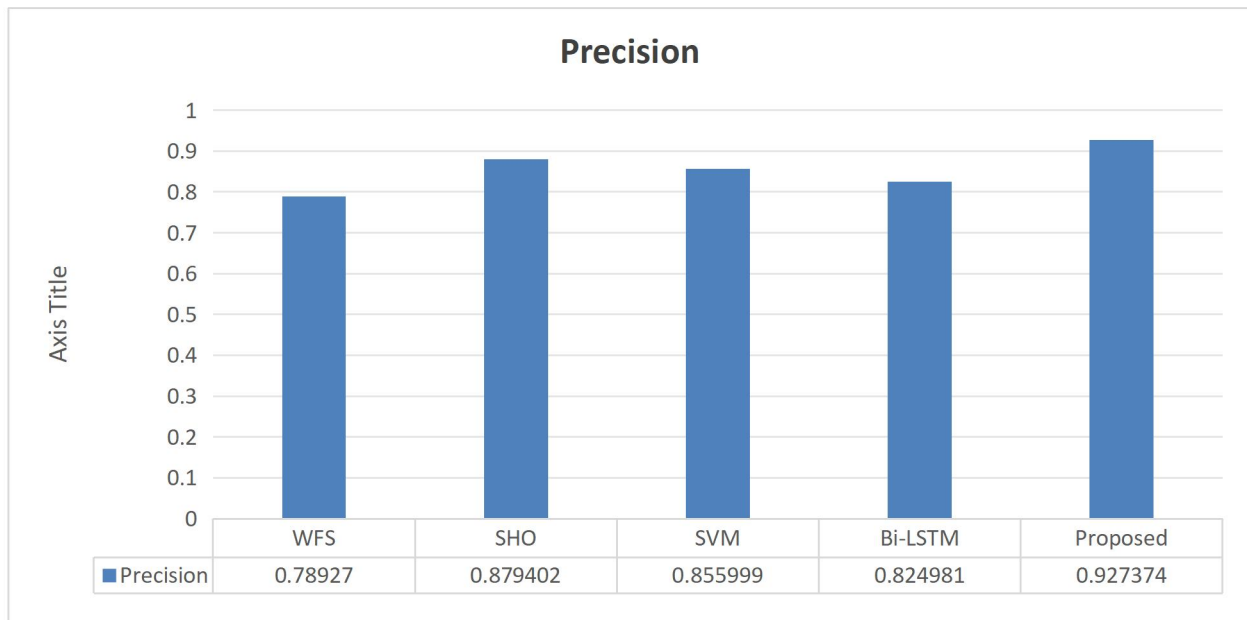

Figure 8:- Precision.

Figure 8 shows the precision analysis. The suggested scheme acquired the best precision score of 0.927374, indicating that it had a high proportion of correct positive predictions. The SHO model also performed well, achieving a precision score of 0.879402. In contrast, the WFS and Bi-LSTM models had lower precision scores of 0.789270 and 0.824981, respectively.
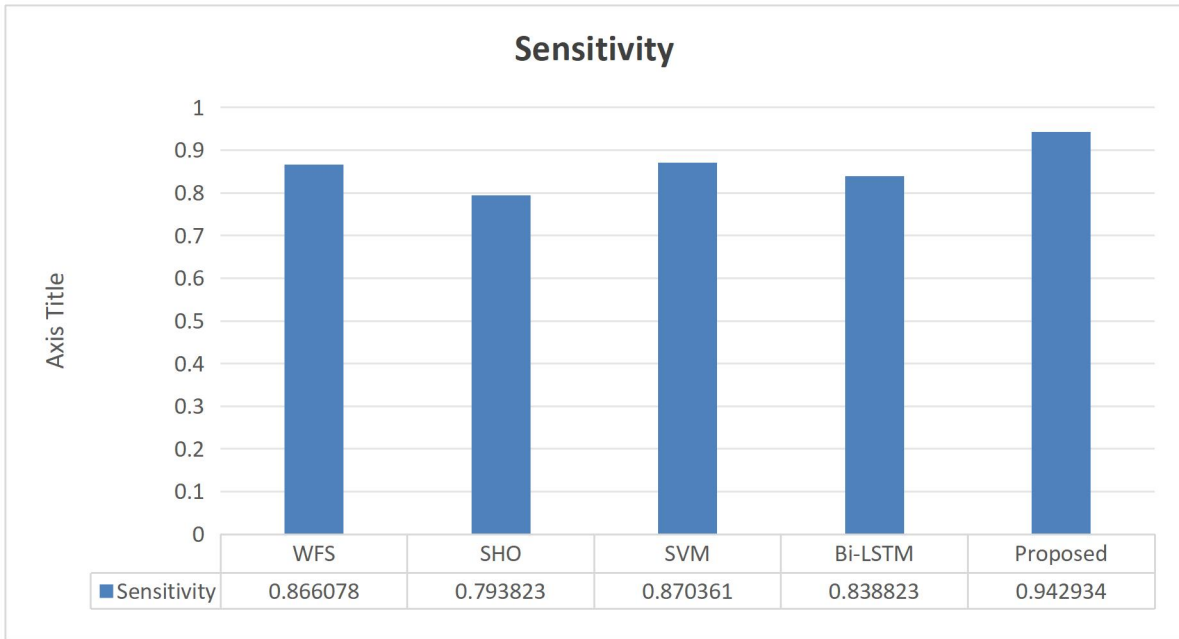
Figure 9:- Sensitivity.

Figure 9 shows the Sensitivity analysis. The suggested scheme obtained the greatest sensitivity of 0.942934 score, indicating that it had a high proportion of correctly identified positive instances. The SVM model also performed well, achieving a sensitivity score of 0.870361. In contrast, the SHO model had the lowest sensitivity score of 0.793823, indicating that it had a lower ability to correctly identify positive instances.
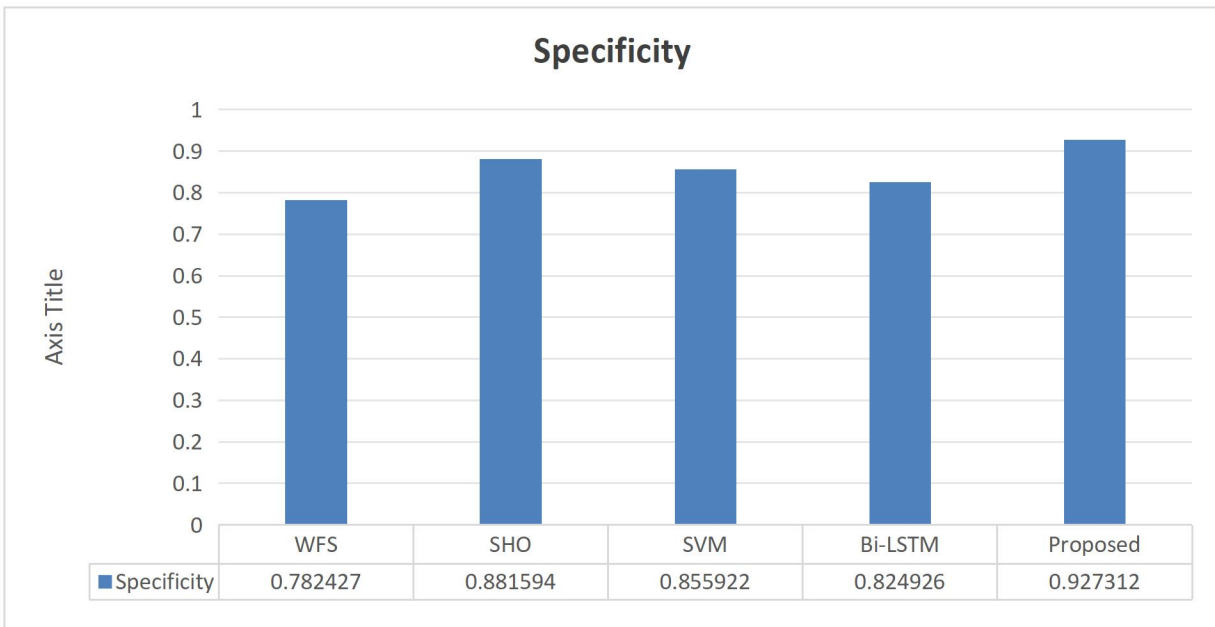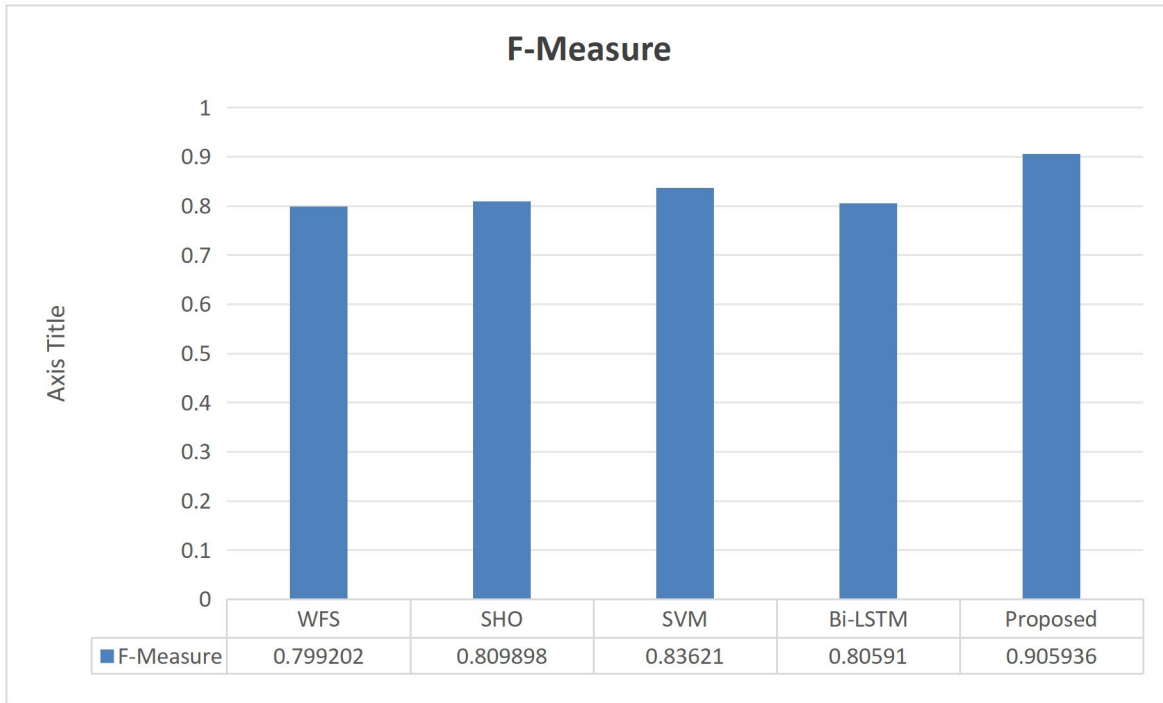

Figure 10:- Specificity.

Figure 10 shows the Specificity analysis. The proposed model also performed well, achieving a specificity score of 0.927312. In contrast, the WFS model had the lowest specificity score of 0.782427, indicating that it had a lower ability to correctly identify negative instances.

Figure 11:- F-Measure.

Figure 11 presents the F-Measure analysis. Proposed model achieved the highest F-measure score of 0.905936. The WFS model had the lowest F-measure score of 0.799202.
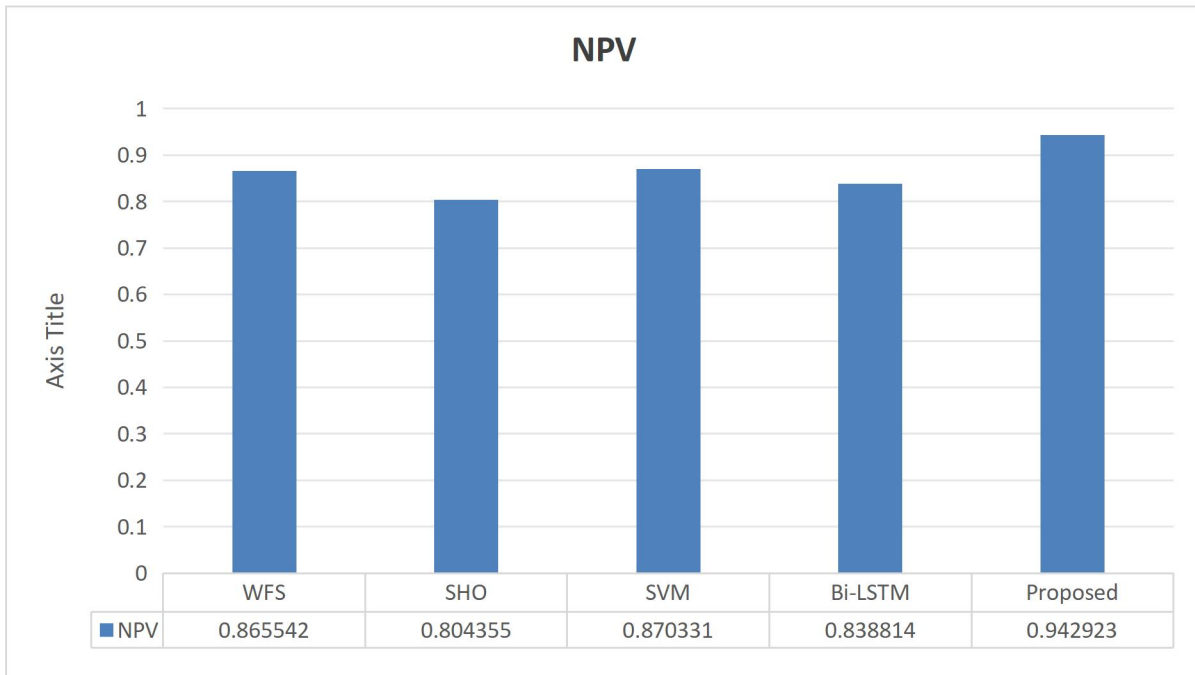
Figure 12:- NPV.

Figure 12 shows the NPV analysis. The highest NPV value of 0.942923 is achieved by the Proposed, which outperforms the other four models by a considerable margin. This indicates that the Proposed model is better at predicting negative outcomes correctly than the other models. The SVM model has the second-highest NPV measure of 0.870331, followed by the WFS model through NPV value of 0.865542. Bi-LSTM and SHO models have similar NPV values of 0.838814 and 0.804355, respectively.
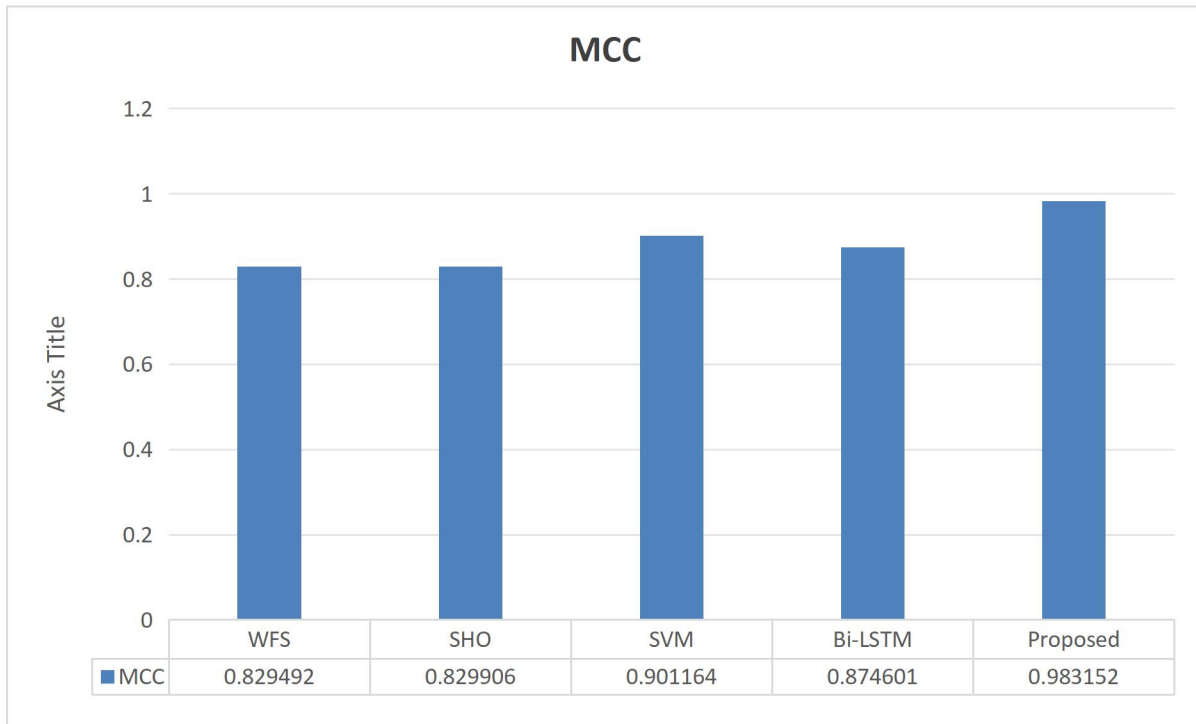
Figure 13:- MCC.

Figure 13 shows the MCC analysis. The highest MCC value of 0.983152 is achieved by the Proposed. This indicates that the Proposed model is better at classifying the data correctly than the other models. The SVM model has the second-highest MCC of 0.901164, tracked by the Bi-LSTM model with MCC evaluate of 0.874601. WFS and SHO models have very similar MCC values of 0.829492 and 0.829906, respectively.
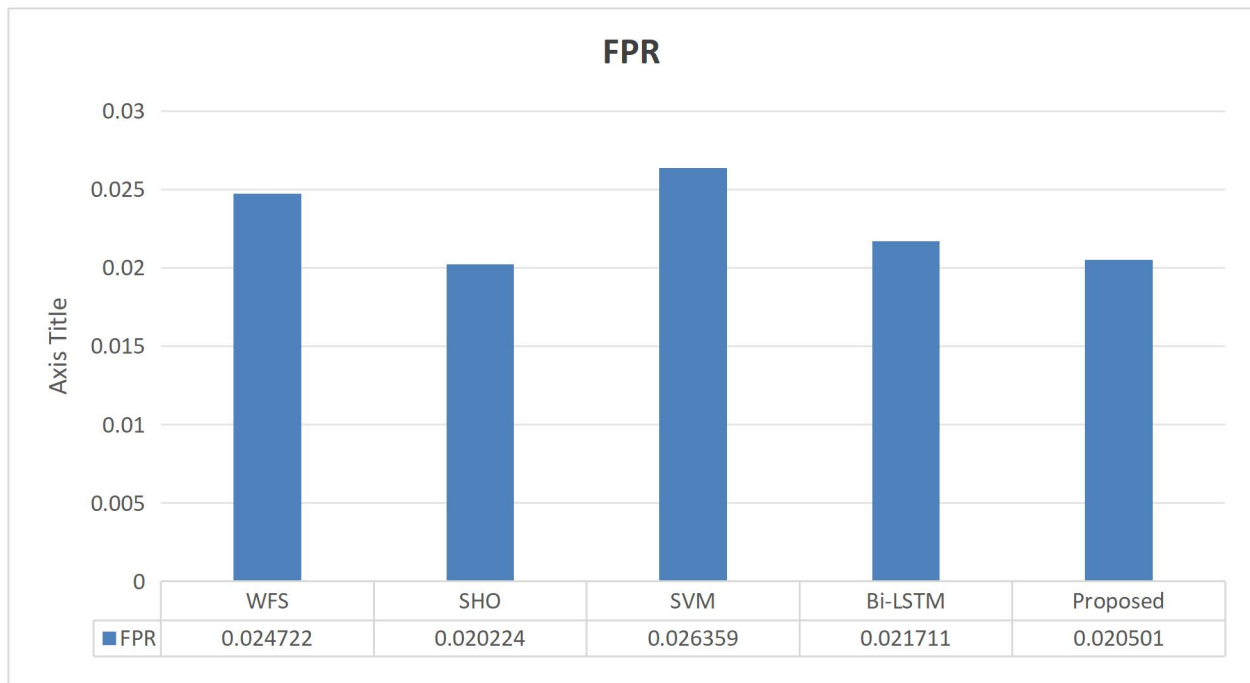

Figure 14:- FPR.

Figure 14 shows the FPR analysis. The FPR values for all five models are relatively low, indicating that the models have a low rate of false positives. Proposed model has FPR of 0.020501. The other three models have slightly higher FPR values, but they are still relatively low.
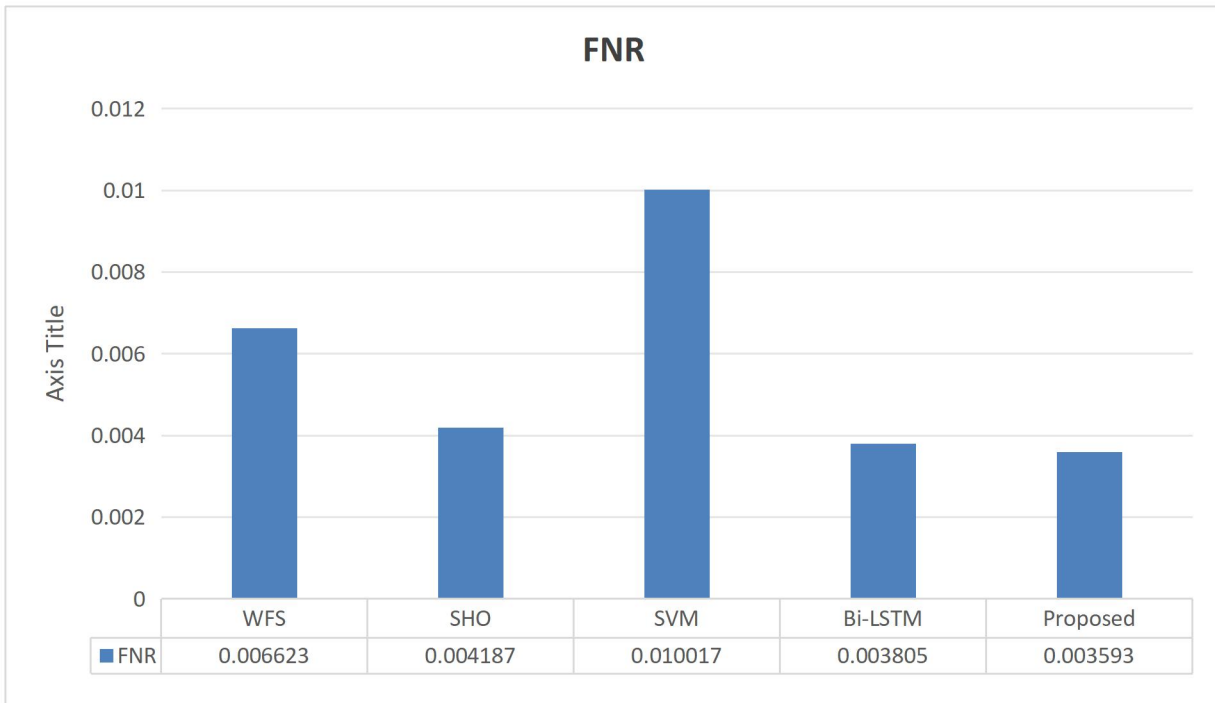
Figure 15:- FNR.

Figure 15 shows the FNR analysis. The FNR values for all five models are low, ranging from 0.003593 to 0.010017. Proposed model has the lowest FNR of 0.003593, followed closely by the Bi-LSTM model with an FNR of 0.003805. The other three models have slightly higher FNR values, but they are still relatively low.

Conclusion:-

This research has successfully established and tested a new metaheuristic algorithm called the Wingsuit Spotted-Hyena Optimizer (WSHO) for selecting the right features and classifying HSIs. Thus, the WSHO model built upon the basis of Wingsuit Flying Search (WFS) and Spotted Hyena Optimizer (SHO) algorithms provides a highly effective solution to the issues raised by high dimensionality and data complexity in hyperspectral analysis. Combining the voice of advanced classifiers like the Support Vector Machine (SVM) and Random Forest (RF) with the proposed Bi-directional Long Short-Term Memory (Bi-LSTM) network has shown considerable enhancement in achievable classifications. The approach also brings the advantage of improving the feature selection and the detection identification of several ground objects.

Through the analysis of a set of complex performance indicators, it has been noted that the effectiveness of the proposed model is significantly higher than that of the traditional methods. This has successfully demonstrated the practical applicability of the WSHO model and how it can be applied practically to identify and categorize different minerals in hyperspectral images. To sum up, it gives the following contributions to information extraction of ground objects from hyperspectral images. Specifically, the proposed WSHO model fulfills important shortcomings of the current methods, which makes the developed approach more correct, effective, and extensible for real-world remote sensing tasks. The work that will be done in the future is to investigate the generalization of this model to some other domains of remote sensing, the improvement of the optimization, and the classification techniques to handle even more complicated data sets.

unwavering support of our families and friends. Their patience and encouragement have been a constant source of motivation.

Data Availability Statement
Dataset is not publicly available. Dataset however available from the authors upon reasonable request and with permission of Author

Authors' Contributions
Gill Ammara & Hongwei Zhang: Conceptualization, Methodology, Data curation, Writing- Original draft preparation, Investigation, Validation, Chang-hua LIU & Xiaojun NIE Visualization, Writing.

Disclosure of potential conflicts of interest
There is no conflict of interest.

Ethical Approval
Approved.

Funding
No funding.

Reference:-

1.   Wang, Z. and Tian, S., 2021. Ground object information extraction from hyperspectral remote sensing images using deep learning algorithm. Microprocessors and Microsystems, 87, p.104394.
2.   Wang, T., & Gan, V. J. (2023). Automated joint 3D reconstruction and visual inspection for buildings using computer vision and transfer learning. Automation in Construction, 149, 104810. https://doi.org/10.1016/j.autcon.2023.104810
3.   Sun, L., Ma, Z., & Zhang, Y. (2023). ABLAL: Adaptive background latent space adversarial learning algorithm for hyperspectral target detection. IEEE Journal of Selected Topics in Applied Earth Observations and Remote Sensing.
4.   Teshome, F. T., Bayabil, H. K., Hoogenboom, G., Schaffer, B., Singh, A., & Ampatzidis, Y. (2023). Unmanned aerial vehicle (UAV) imaging and machine learning applications for plant phenotyping. Computers and Electronics in Agriculture, 212, 108064.
5.   Storch, T., Honold, H. P., Chabrillat, S., Habermeyer, M., Tucker, P., Brell, M., ... & Fischer, S. (2023). The EnMAP imaging spectroscopy mission towards operations. Remote Sensing of Environment, 294, 113632.
6.   Guo, X., Lao, J., Dang, B., Zhang, Y., Yu, L., Ru, L., ... & Li, Y. (2024). Skysense: A multi-modal remote sensing foundation model towards universal interpretation for earth observation imagery. In Proceedings of the IEEE/CVF Conference on Computer Vision and Pattern Recognition (pp. 27672-27683).
7.   Sikakwe, G. U. (2023). Mineral exploration employing drones, contemporary geological satellite remote sensing and geographical information system (GIS) procedures: A review. Remote Sensing Applications: Society and Environment, 31, 100988.
8.   Sudmanns, M., Augustin, H., Killough, B., Giuliani, G., Tiede, D., Leith, A., ... & Lewis, A. (2023). Think global, cube local: an Earth Observation Data Cube's contribution to the Digital Earth vision. Big Earth Data, 7(3), 831-859.
9.   Asif, S., Wenhui, Y., ur-Rehman, S., ul-ain, Q., Amjad, K., Yueyang, Y., ... & Awais, M. (2024). Advancements and Prospects of Machine Learning in Medical Diagnostics: Unveiling the Future of Diagnostic Precision. Archives of Computational Methods in Engineering, 1-31.
10. Otgonbaatar, S. and Datcu, M., (2021). A quantum annealer for subset feature selection and the classification of hyperspectral images. IEEE Journal of Selected Topics in Applied Earth Observations and Remote Sensing, 14, pp.7057-7065.
11. Xie, Z., Duan, P., Liu, W., Kang, X., Wei, X., & Li, S. (2023). Feature consistency-based prototype network for open-set hyperspectral image classification. IEEE Transactions on Neural Networks and Learning Systems.
12. Dai, Q., Ishfaque, M., Khan, S.U.R. et al. Image classification for sub-surface crack identification in concrete dam based on borehole CCTV images using deep dense hybrid model. Stoch Environ Res Risk Assess (2024). https://doi.org/10.1007/s00477-024-02743-x
13. Zhao, Z., Hu, D., Wang, H. and Yu, X., 2021. Center attention network for hyperspectral image classification. IEEE Journal of Selected Topics in Applied Earth Observations and Remote Sensing, 14, pp.3415-3425.

14. Chen, Y., Wang, Y., Gu, Y., He, X., Ghamisi, P. and Jia, X., 2024. Deep learning ensemble for hyperspectral image classification. IEEE Journal of Selected Topics in Applied Earth Observations and Remote Sensing, 12(6), pp.1882-1897.
15. Khan, S.U.R.; Zhao, M.; Asif, S.; Chen, X. Hybrid-NET: A fusion of DenseNet169 and advanced machine learning classifiers for enhanced brain tumor diagnosis. Int. J. Imaging Syst. Technol. 2024, 34, e22975.
16. Asif, S., Zhao, M., Li, Y., Tang, F., Ur Rehman Khan, S., & Zhu, Y. (2024). AI-Based Approaches for the Diagnosis of Mpox: Challenges and Future Prospects. Archives of Computational Methods in Engineering, 1-33.
17. Huang, Y., Peng, J., Ning, Y., Sun, W. and Du, Q., 2021. Graph embedding and distribution alignment for domain adaptation in hyperspectral image classification. IEEE Journal of Selected Topics in Applied Earth Observations and Remote Sensing, 14, pp.7654-7666.
18. Zhou, Y., Huo, H., Hou, Z., & Bu, F. (2023). A deep graph convolutional neural network architecture for graph classification. Plos One, 18(3), e0279604.
19. Khan, S. U. R., Asif, S., Bilal, O., & Ali, S. (2024). Deep hybrid model for Mpox disease diagnosis from skin lesion images. International Journal of Imaging Systems and Technology, 34(2), e23044.
20. Finn, A., Peters, S., Kumar, P., & O'Hehir, J. (2023). Automated Georectification, Mosaicking and 3D Point Cloud Generation Using UAV-Based Hyperspectral Imagery Observed by Line Scanner Imaging Sensors. Remote Sensing, 15(18), 4624.
21. Shen, L., Lang, B., & Song, Z. (2023). DS-YOLOv8-Based object detection method for remote sensing images. Ieee Access, 11, 125122-125137.
22. Li, X., Li, Z., Qiu, H., Hou, G., & Fan, P. (2023). An overview of hyperspectral image feature extraction, classification methods and the methods based on small samples. Applied Spectroscopy Reviews, 58(6), 367-400.Xue, Z., Liu, Z., & Zhang, M. (2023). DSR-GCN: Differentiated-scale restricted graph convolutional network for few-shot hyperspectral image classification. IEEE Transactions on Geoscience and Remote Sensing, 61, 1-18.
23. Han, C., Wu, C., Guo, H., Hu, M., & Chen, H. (2023). HANet: A hierarchical attention network for change detection with bitemporal very-high-resolution remote sensing images. IEEE Journal of Selected Topics in Applied Earth Observations and Remote Sensing, 16, 3867-3878.
24. Alam, M.M., Hamida, E.B., Berder, O., Menard, D. and Sentieys, O., 2022. A heuristic self-adaptive medium access control for resource-constrained. WBAN systems. IEEE Access, 4, pp.1287-1300.
25. Zhang, Z., Ma, Q., Zhou, H. and Gong, N., 2022. Nested Transformers for Hyperspectral Image Classification. Journal of Sensors, 2022.
26. Hang, R., Li, Z., Liu, Q., Ghamisi, P. and Bhattacharyya, S.S., 2020. Hyperspectral image classification with attention-aided CNNs. IEEE Transactions on Geoscience and Remote Sensing, 59(3), pp.2281-2293.
27. Das, D., Biswas, S. K., & Bandyopadhyay, S. (2023). Detection of diabetic retinopathy using convolutional neural networks for feature extraction and classification (DRFEC). Multimedia Tools and Applications, 82(19), 29943-30001.
28. Renlong Hang, Zhu Li, et.al., (2020). Hyperspectral Image Classification with Attention Aided CNNs. Remote Sensing, pp.12.
29. Yanhui Guo et al. (2018), High Efficient Deep Feature Extraction and Classification of Spectral-Spatial HIS. Remote Sensing, pp.13.